Mesoporous Carbon Spheres

DOI: 10.1002/ange.201407629

Synthesis of Nitrogen-Doped Mesoporous Carbon Spheres with Extra-Large Pores through Assembly of Diblock Copolymer Micelles**

Jing Tang, Jian Liu, Cuiling Li, Yunqi Li, Moses O. Tade, Sheng Dai,* and Yusuke Yamauchi**

Abstract: *The synthesis of highly nitrogen-doped mesoporous carbon spheres (NMCS) is reported. The large pores of the NMCS were obtained through self-polymerization of dopamine (DA) and spontaneous co-assembly of diblock copolymer micelles. The resultant narrowly dispersed NMCS possess large mesopores (ca. 16 nm) and small particle sizes (ca. 200 nm). The large pores and small dimensions of the N-heteroatom-doped carbon spheres contribute to the mass transportation by reducing and smoothing the diffusion pathways, leading to high electrocatalytic activity.*

Porous carbon materials have unique characteristics, such as a good electrical conductivity, chemical inertness, high surface area, large porosity, and good biocompatibility, thereby showing many potential applications in a wide range of research fields (e.g. adsorption, energy conversion and storage, catalysis, and sensor technology).[1] As demonstrated in many studies, mesoporous materials show an excellent performance compared to microporous materials, because of the less limited diffusion. Using mesopores, especially large-sized mesopores, smooth mass transport can be realized for large reagent molecules.[2] The morphological control is also a critical factor. The spherical morphology attracts sustained research interests especially when the particle size is smaller than 200 nm, because it provides short pathways for mass transport and minimizes the viscous effects.[3] Several successful applications in drug delivery, gene therapy, supercapacitors, Li-S batteries, and CO_2 capture have been reported by using spherical carbon materials, due to their inherent short diffusion path way and the effective intracellular endocytosis.[4]

So far, various porous carbon spheres have been prepared using different methods, including a Stöber-based method, hard- and soft-templating methods, and a direct polymerization method.[5] For example, microporous carbon spheres with particle sizes from 120 to 800 nm have been synthesized through direct self-polymerization and subsequent carbonization by Lu and co-workers.[6a] Although the resultant carbon spheres have a high surface area after treatment with KOH, the pores in the spheres are still micropores with a pore size smaller than 2 nm. Zhao et al. developed a hydrothermal method for the synthesis of ordered mesoporous carbon spheres derived from co-assembly of resol and F127.[6b] However, their pore sizes are still limited to 3 nm. Therefore, such a limitation on the pore size in carbon spheres significantly devalues their practical applications.

Until now, mesoporous materials with pore size larger than 10 nm have been successfully prepared by using various high-molecular-weight block polymers, such as polystyrene-*block*-poly(ethylene oxide) (PS-*b*-PEO), polyisobutylene-*block*-PEO (PIB-*b*-PEO), PS-*block*-poly(4-vinylpyridine) (PS-*b*-P4VP), and PEO-*block*-poly(methyl methacrylate) (PEO-*b*-PMMA) as soft templates. However, they are mostly used in the form of films or irregulary shaped particles with micrometer sizes.[7] These systems are based on solvent evaporation processes which are not applicable to prepare mesoporous carbon spheres. Mesoporous carbon spheres with large-sized pores will lead to many applications which are not attainable by films and irregular particles, as mentioned above.

By using the micelles of a high-molecular-weight block polymer PS-*b*-PEO as a template, we propose a facile micelle route for the preparation of N-doped mesoporous carbon spheres (NMCS) with large mesopore sizes (up to 16 nm), as shown in Figure 1. The resultant mesoporous carbon spheres are promising catalysts for the oxygen reduction reaction (ORR) and also would show promising applications in large biomolecule adsorption and gene therapy. The key of our synthesis is the use of DA/PS-*b*-PEO composite micelles which are stably pre-formed in the reaction solution. Polymerization of the DA molecules and further co-assembly with the PS-*b*-PEO micelles result in the formation of PDA/PS-*b*-PEO composite spheres (where polymerized dopamine is abbreviated as PDA). The PS-*b*-PEO micelles acting as

[*] J. Tang, Dr. C. Li, Y. Li, Prof. Y. Yamauchi
World Premier International (WPI) Research Center for Materials Nanoarchitectonics (MANA)
National Institute for Materials Science (NIMS)
1-1 Namiki, Tsukuba, Ibaraki 305-0044 (Japan)
E-mail: Yamauchi.Yusuke@nims.go.jp
Homepage: http://www.yamauchi-labo.com
J. Tang, Y. Li, Prof. Y. Yamauchi
Faculty of Science and Engineering, Waseda University
3-4-1 Okubo, Shinjuku, Tokyo 169-8555 (Japan)
Dr. J. Liu, Prof. M. O. Tade
Department of Chemical Engineering, Curtin University
Perth, Western Australia 6845 (Australia)
E-mail: jian.liu@curtin.edu.au
Prof. S. Dai
Department of Chemistry, University of Tennessee
Knoxville, TN 37996 (USA)
E-mail: sdai@utk.edu

[**] We acknowledge kind help on XPS analysis from Dr. Hideo Iwai and Dr. Akihiro Tanaka in Materials Analysis Station, NIMS. J.L. gratefully acknowledges the support of JSPS Invitation Fellowship. S.D. is supported as part of the Fluid Interface Reactions, Structures and Transport (FIRST) Center, an Energy Frontier Research Center funded by the US Department of Energy, Office of Science, Office of Basic Energy Sciences.

Supporting information for this article is available on the WWW under http://dx.doi.org/10.1002/anie.201407629.

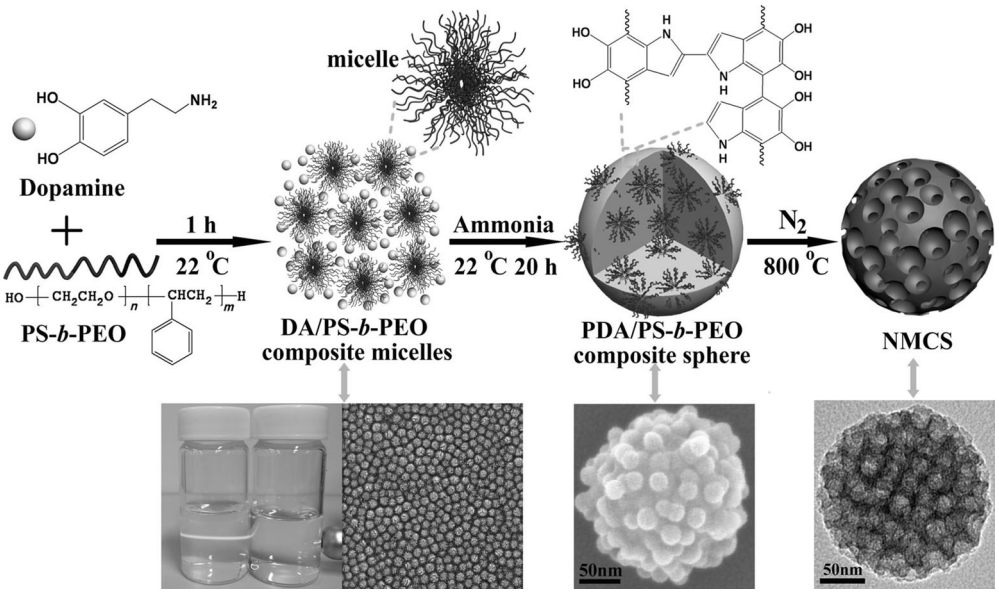

Figure 1. Formation process of the N-doped mesoporous carbon nanospheres (NMCS).

a sacrificial pore-forming agent are removed during the carbonization process, leaving the mesopores in the carbon spheres.

DA is used as both carbon and nitrogen sources in this study, which is critically important for high doping of N heteroatoms in the carbon matrix. Although DA has been often used for the preparation of N-doped carbon materials, microporous and/or non-porous carbon compounds have been always obtained through these methods.[6a,8] It is difficult to control the pore sizes by using surfactants, probably because of the weak interaction between DA molecules and low-molecular-weight block copolymer or ionic surfactants. Carbon nanomaterials doped with heteroatoms, such as nitrogen, boron, and sulfur, have attracted much attention, because of their modification of electron donor/acceptor characteristics and the resulting enhancement of electrochemical properties.[9] N-doped carbon nanomaterials, such as N-doped nanotubes, graphene, and mesoporous carbon, have shown superior electrocatalytic performance and good stability for the ORR. Therefore, the large pore-sized NMCS reported here would surely contribute to mass transportation by reducing and smoothing the diffusion pathways, which are expected to lead to high electrocatalytic activity for the ORR. These studies will provide not only a new synthesis method, but also important insight into designing mesoporous carbon spheres for various applications.

Figure 2 a–d shows scanning electron microscope (SEM) images for PDA spheres prepared without using PS-*b*-PEO micelles and PDA/PS-*b*-PEO composite spheres prepared by employing three PS-*b*-PEO diblock copolymers with different polymerization degree of PS and PEO chains, namely, PS_{37}-*b*-PEO_{114}, PS_{178}-*b*-PEO_{886}, and PS_{173}-*b*-PEO_{170}. All the composite spheres show uniform particle sizes and shapes, and their average particle sizes are 194, 180, 255, and 203 nm for PDA spheres, PDA/PS_{37}-*b*-PEO_{114}, PDA/PS_{178}-*b*-PEO_{886}, and PDA/PS_{173}-*b*-PEO_{170} composite spheres, respectively, as shown in low-magnified SEM images (Figure S1). The PDA spheres prepared without PS-*b*-PEO micelles have a very smooth surface (Figure 2 a), while clear round bumps are observed on the surface of PDA/PS-*b*-PEO composite spheres (Figure 2 b–d and Figure S2). The bumpiness on the particle surface is obviously increased by using the diblock copolymer with longer PS chains. When using PS_{173}-*b*-PEO_{170} as a template, the micelles as a template are more clearly confirmed (Figure 2 d).

After heat treatment at 800 °C in N_2 atmosphere (i.e., carbonization), the PDA/PS-*b*-PEO composite spheres were converted to

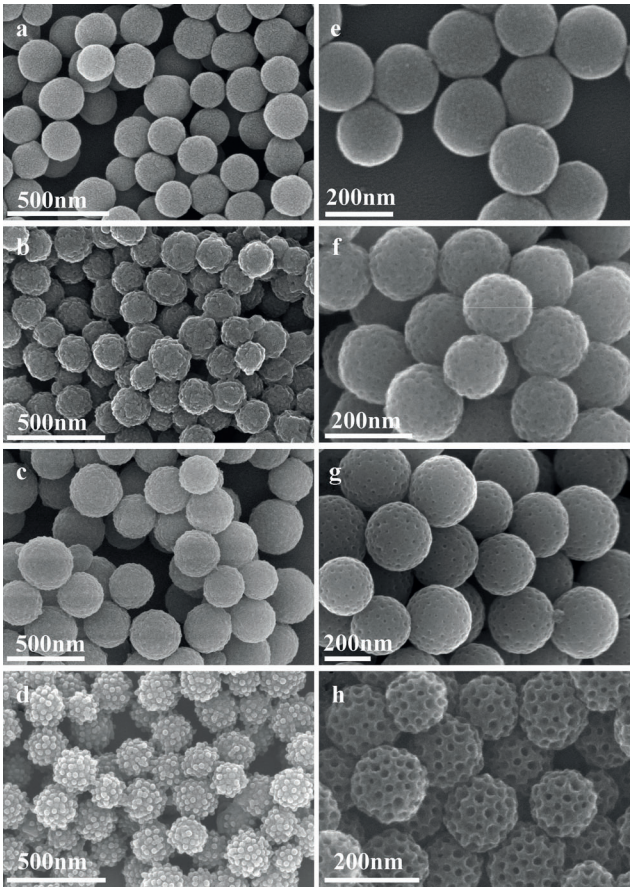

Figure 2. a–d) SEM images of a) PDA spheres, b) PDA/PS_{37}-*b*-PEO_{114} composite spheres, c) PDA/PS_{178}-*b*-PEO_{886} composite spheres, and d) PDA/PS_{173}-*b*-PEO_{170} composite spheres. e–h) SEM images of the corresponding N-doped carbon spheres (NCS) and N-doped mesoporous carbon spheres (NMCS) carbonized at 800 °C for e) NCS, f) NMCS-1, g) NMCS-2, and h) NMCS-3.

NMCS. Three types of NMCS were prepared from PDA/PS_{37}-*b*-PEO_{114}, PDA/PS_{178}-*b*-PEO_{886}, and PDA/PS_{173}-*b*-PEO_{170} composite spheres. These samples are denoted as NMCS-1, NMCS-2, and NMCS-3, respectively. For comparison, PDA spheres prepared without using PS-*b*-PEO micelle were also thermally converted to N-doped carbon spheres (NCS) without mesopores. The original spherical morphology is completely retained without formation of cracks and holes. The sizes of NMCS are decreased compared with the PDA/PS-*b*-PEO composite spheres before the carbonization (Figure S3). Uniformly sized mesopores are well distributed on the sphere surface and their mesopore sizes roughly estimated from SEM images distinctly expanded from 5 to 16 nm by increasing the PS chain lengths (Figure 2 f–h). The lengths (i.e., molecular weights) of the PS chains strongly influence the pore sizes in the final NMCS, which will be discussed later. Focused ion-beam scanning electron microscopy (FIB-SEM) shows that uniformly sized mesopores existed in both the exterior and interior of the carbon spheres (Figure S4). The spherical morphology and large-sized mesoporous structure in the NMCS still remain intact even extending the carbonization temperature to 1000 °C, showing good structural stability (Figure S5).

As revealed by TEM images (Figure S6), the PDA/PS-*b*-PEO composite spheres (Figure S6 b–d) have rough surfaces compared with PDA spheres (Figure S6 a), which corresponds with the SEM results (Figure 2 a–d). NMCS carbonized from PDA/PS-*b*-PEO composite spheres show distinct mesopores throughout the whole spheres (Figure S6 f–h). Nitrogen adsorption–desorption isotherms were measured to investigate the porosities of both NCS and NMCS. The isotherms of the NCS are type I isotherms (Figure S7A). The high N_2 adsorption shown in the adsorption branch at a relative low pressure is typically associated with micropores. Thus, without the templates, the carbonization in the polymeric matrix causes the formation of micropores because of the generation of gas in the spheres, which has been reported previously.[6a] In contrast, NMCS-1, NMCS-2, and NMCS-3 show type IV isotherms with hysteresis loops. This behavior is typically associated with the capillary condensation of N_2 into the mesopores. The Brunauer–Emmett–Teller (BET) surface areas, total pore volumes, and average pore sizes are summarized in Table 1. From the pore size distribution curves (Figure S7B), it is demonstrated that NMCS possess uniformly sized mesopores. The average pore size of NMCS-1 is 5.4 nm, while those of NMCS-2 and NMCS-3 are as large as 16.0 nm. These values are almost the same as those observed by SEM (Figure 2 f–h).

Based on the above observation, we propose the formation mechanism, as described in Figure 1. In the experimental process, PS-*b*-PEO was firstly mixed in THF solution, in which it was completely dissolved and existed as a unimer. After adding water and ethanol, the micellization process occurred, in which the Tyndall effect was clearly observed (Figure S8a). As a typical example, the SEM image of the PS_{173}-*b*-PEO_{170} micelle solution shows the presence of the diblock polymer micelles with a diameter of around 20 nm (Figure S8b), which is exactly the same micelles size observed in Figure S2d. After addition of DA, the DA species surrounded the micelle surface by hydrogen bonding between the catechol and the N-H groups in DA and -OH group in the PEO block.[10] According to a zeta-potential measurement, the DA/PS-*b*-PEO composite micelles were slightly positive charged, thereby further inducing a good dispersion of micelles (Figure S8c). The SEM image in Figure S8c also indicates the existence of well-dispersed DA/PS-*b*-PEO composite micelles. After adding ammonia solution, the polymerization reaction of DA molecules proceeds under alkaline condition.[10a,b,11] During this stage, the DA/PS-*b*-PEO composite micelles are self-assembled and polymerized to form PDA/PS-*b*-PEO composite spheres, as shown in Figure 1. The PDA still strongly interacts with the PS-*b*-PEO template because of the catechols/quinone groups present in the PDA.[10a,b] After 2 h of reaction, small-sized PDA/PS-*b*-PEO composite spheres (with an average size of 185 nm) are formed (Figure S9a). With increase of the reaction time, the average particle sizes gradually grow to 378 nm (Figure S9b–d). In our approach, the PS-*b*-PEO micelles act as a sacrificial pore-forming agent during carbonization. The mesopore sizes observed on the surface of the NMCS are slightly smaller than the micelle sizes observed on the original PDA/PS-*b*-PEO composite spheres (Figure S2), due to thermal shrinkage of the pore walls.

The detailed carbonization process along with the weight loss of PDA spheres and PDA/PS-*b*-PEO composite spheres were investigated by thermogravimetric (TG) analysis (Figure S10 and Table S1). The PDA spheres show a good thermal stability, in which the residues remain 76.2 % at 350 °C because of the loss of functional groups, and then illustrate a satisfied carbonization yield of 50.9 % at 1000 °C. On the other hand, the carbonization yields for PDA/PS_{37}-*b*-PEO_{114}, PDA/PS_{178}-*b*-PEO_{886}, and PDA/PS_{173}-*b*-PEO_{170} composite spheres are 46.9, 43.1, and 30.8 wt %, respectively. PDA/PS-*b*-PEO composite spheres display a larger mass decrease and less residues at 350 °C. Compared with PDA spheres, the extra weight loss of PDA/PS_{37}-*b*-PEO_{114}, PDA/PS_{178}-*b*-PEO_{886}, and PDA/PS_{173}-*b*-PEO_{170} at 350 °C are 6.40, 11.5, and 24.7 wt %, respectively. Nevertheless, they illustrate similar weight loss (ca. 21 wt %) from 350 to 1000 °C (Table S1). These results suggest that the extra weight loss of PDA/PS-*b*-PEO composite spheres at 350 °C is probably due to the removal of PS-*b*-PEO micelles with different molecular weights of the PS and PEO blocks. As revealed by SEM images of PDA/PS_{173}-*b*-PEO_{170} composite spheres carbonized from 300 to 350 °C, the micelles on the surface gradually disappear and finally they are completely removed at 350 °C (Figure S11).

Table 1: Physicochemical properties and average particle sizes of NMCS-1, NMCS-2, and NMCS-3 samples.

Sample	Surface area [$m^2 g^{-1}$]	Pore volume [$cm^3 g^{-1}$]	Pore size [nm]	Particle size [nm]
NMCS-1	363	0.48	5.4	165
NMCS-2	356	0.45	16.0	201
NMCS-3	343	0.48	16.0	180

As mentioned in Figure 2, the PS core sizes in the micelles determine the pore sizes in the obtained NMCS. In addition to NMCS-1, NMCS-2, and NMCS-3, we prepared another two kinds of NMCS using PS_{31}-*b*-PEO_{284} and PS_{87}-*b*-PEO_{227} as the templates. The pore sizes were determined by N_2 adsorption–desorption measurement (Figure S12). Notably, the increase of the molecular weight of the PS blocks leads to a gradual expansion of the pore sizes (Figures S13 and S14). In addition, the PEO blocks (i.e., shell region of micelles) are interacting with the DA and PDA, in which the PEO shell thickness basically influences the wall thickness in the NMCS. Among the used five block copolymers, PS_{173}-*b*-PEO_{170} shows the highest weight ratio of PS/PEO. Therefore, the resulting NMCS-3 possess a relatively thin wall thickness and the mesopores are more closely packed inside the spheres, compared to the others (Figure S14).

X-ray photoelectron spectroscopy (XPS) analysis was performed to determine the electric state of the N content. Both PDA/PS_{173}-*b*-PEO_{170} composite spheres (before carbonization) and corresponding NMCS-3 (after carbonization) were measured, as shown in Figure 3 A. The N1s spectrum of the PDA/PS_{173}-*b*-PEO_{170} composite sphere shows one peak centered at 399.8 eV which is attributed to the pyrrole N.[12] After carbonization, the N1s spectrum of NMCS-3 is deconvoluted into two binding energies centered at 398.4[12,13] and 400.8 eV,[14] which can be assigned to pyridinic N and graphitic N, respectively. The presence of N atoms in NMCS-3 was further confirmed by the elemental mapping analysis (Figure 3 B). The content of C and N in NMCS-3 detected by elemental analysis is 92.3 wt% and 7.6 wt%, respectively, which matches with the XPS data. The N content in the other NCS, NMCS-1, and NMCS-2 samples measured by elemental analysis are 7.7, 7.3 and 7.5 wt%, respectively (Figure S15). There is no large difference of the N content among the samples.

Toward development of new energy system, researchers are searching for efficient nonprecious metal catalysts or metal-free catalysts as substitution of Pt for the oxygen reduction reaction which is intrinsically sluggish but important in the cathodic reaction. Doping of electron-accepting N atoms in the carbon plane, especially graphitic N and pyridinic N species, is critical for the ORR by imparting higher positive charge density on adjacent carbon atoms and weakening the O–O bond.[15] During the ORR, oxygen can be activated by direct bonding with the lone pair electrons of pyridinic N atoms.[15d] And, the graphitic N atoms promote the ORR by electron transfer from the carbon electronic bands to the antibonding orbitals of O_2 and facilitating O_2 dissociation on the adjacent C atoms.[15e] Here we evaluated the ORR activity of the NCS and NMCS samples by measuring linear-sweep voltammograms (LSVs) in O_2-saturated 0.1 M KOH solution using a rotating disk electrode (RDE). To emphasize the importance of our materials, the commercially available Pt catalyst (20 wt% was also measured as a reference.

The onset potentials of NCS, NMCS-1, NMCS-2, NMCS-3, and Pt/C were −0.15, −0.13, −0.12, −0.11, and −0.07 V, respectively, and the limiting currents were 3.14, 3.40. 4.35, 5.56, and 5.37 mA cm^{-2}, respectively (Figure 3 C and Figure S16). Clearly, NMCS with large mesopores show a more positive onset potential and a higher diffusion-limited current, compared to NCS with micropores, indicating their better electrocatalytic activity for the ORR. The improved electrochemical performance of NMCS is a result of their sufficient accessible porous architecture, which can reduce the diffusion resistance and enhance the three-phase boundary of gas, electrolyte, and solid catalyst.[16] Interestingly, NMCS-3 exhibit a similar diffusion-limited current for the ORR compared with Pt/C, although the onset potential is slightly negative. Cyclic voltammography curves of NMCS-3, performed in N_2- and O_2-saturated 0.1 M KOH solution (Figure S17), presents a distinct cathodic ORR peak at −0.21 V after introducing O_2, further demonstrating the pronounced electrocatalytic activity of NMCS-3 towards the ORR. The electron transfer number involved in NMCS-3 for the ORR was estimated to be 3.4 from the slope of the Koutecky–Levich plots (Figure S18) and was further verified by a rotating ring-disk electrode (RRDE; Figure 3 D) test. The corre-

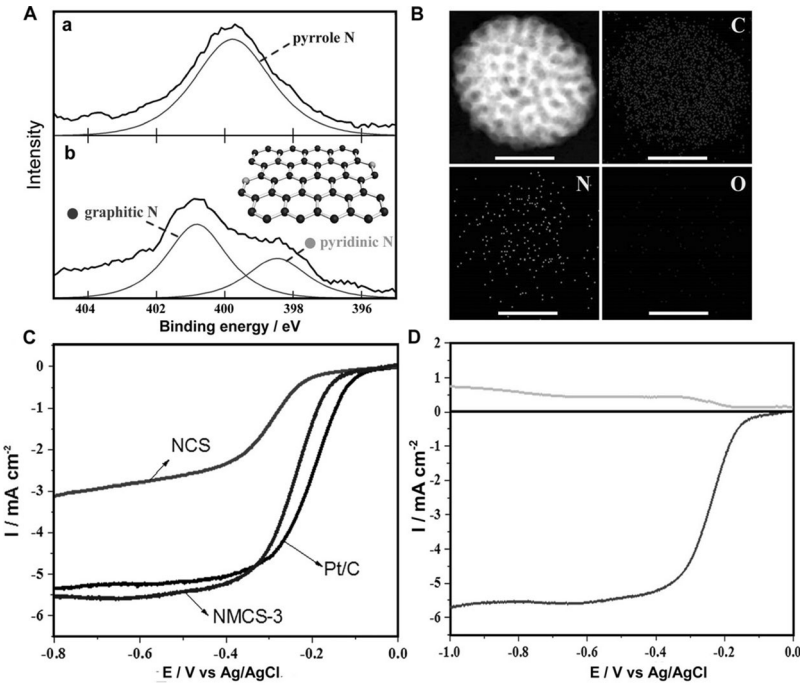

Figure 3. A) The high-resolution N1s XPS spectrum of a) PDA/PS_{173}-*b*-PEO_{170} composite spheres and b) NMCS-3. The inset shows a schematic illustration of the nitrogen atoms in NMCS-3. B) HAADF-STEM image and elemental mapping of NMCS-3. The scale bar is 100 nm. C) Polarization curves of NCS, NMCS-3, and Pt/C catalyst in O_2-saturated 0.1 M KOH solutions with a scan rate of 10 mV s^{-1} and a rotating rate of 1600 rpm. D) Rotating ring-disk electrode (RRDE) test of the ORR on NMCS-3 in an O_2-saturated 0.1 M KOH electrolyte at a scan rate of 10 mV s^{-1}. The rotation rate is 1600 rpm and the Pt ring electrode is poised at 1.0 V for oxidizing HO_2^- intermediate.

sponding amperometric current (upper curve in Figure 3D) for the oxidation of hydrogen peroxide ions (HO_2^-) was recorded at the Pt ring electrode. The results indicate that the ORR using NMCS-3 involves both two-electron and four-electron reactions, which is common in N-doped metal-free carbon materials.[15a,16e,17]

The durability of the catalyst is another major concern in fuel-cell technology. We further investigated the stability of NMCS-3 and Pt/C by using the *i–t* chronoamperometric measurement at a constant voltage of −0.6 V in O_2-saturated 0.1M KOH with rotation rate of 1600 rpm. Both the catalysts display a high transient current which fast degrades within the first 10 s. Then, NMCS-3 presented less current loss (84%) at steady state than Pt/C (76%). Thus, it is proved that the durability of NMCS-3 is superior to that of the Pt/C catalyst.

In addition, we investigated the effect of the carbonization temperature on ORR activity. For this purpose, we carbonized the representative NMCS-3 at various temperatures from 700 to 1000°C (Figure S19–S22). The physicochemical properties and element composition changes in NMCS are concluded in Table S2 and Figure S23. The ORR activity was measured by using RDE in O_2-saturated 0.1M KOH solution (Figure S24). Remarkably, the NMCS-3 carbonized at 900°C exhibit the best catalytic activity for ORR with more positive onset potential and highest current density (Figure S24), due to its balance between the graphitization degree, specific surface area, and electrochemically active N species.[15b,c] Compared with other metal-free carbon-based materials (Table S3), NMCS-3 has become one of the most active metal-free N-doped carbon catalysts towards ORR.[6a,16e,18]

In conclusion, our present synthesis is based on co-assembly of diblock polymer PS-*b*-PEO micelles and non-toxic DA as the carbon and nitrogen sources. The use of DA offers a simple route for in situ introducing heteroatoms with high content into carbon materials. To the best of our knowledge, there have been no reports on highly N-doped mesoporous carbon spheres with extra-large mesopores (up to 16 nm). Both large-sized mesopores and high N-doping are very effective for acceleration of the ORR. Our NMCS realize high electrocatalytic activity and excellent long-term stability towards the ORR, even comparable to the Pt/C catalyst. These results shed light on the synthesis of mesoporous carbon spheres for various applications in the emerging field. By further optimization of porous architectures and compositions, we can expect to realize promising materials as cathode electrode.[19] Moreover, by selecting other carbon sources which effectively interact with the micelle surface, various large-sized mesoporous carbons with different heteroatoms are expected for improving the capacitance,[8b] surface polarity, and basic sites.[20]

Received: July 25, 2014
Revised: October 6, 2014
Published online: November 12, 2014

Keywords: carbon spheres · large-sized mesopores · mesoporous materials · micelles · oxygen reduction reaction

[1] a) C. D. Liang, Z. J. Li, S. Dai, *Angew. Chem. Int. Ed.* **2008**, *47*, 3696; *Angew. Chem.* **2008**, *120*, 3754; b) Z. X. Wu, W. D. Wu, W. J. Liu, C. Selomulya, X. D. Chen, D. Y. Zhao, *Angew. Chem. Int. Ed.* **2013**, *52*, 13764; *Angew. Chem.* **2013**, *125*, 14009; c) W. Luo, B. Wang, C. G. Heron, M. J. Allen, J. Morre, C. S. Maier, W. F. Stickle, X. L. Ji, *Nano Lett.* **2014**, *14*, 2225; d) T. Y. Ma, J. R. Ran, S. Dai, M. Jaroniec, S. Z. Qiao, *Angew. Chem. Int. Ed.* **2014**, *53*, 7281; *Angew. Chem.* **2014**, *126*, 7409; e) Y. Zheng, Y. Jiao, L. H. Li, X. Tan, Y. Chen, M. Jaroniec, S. Z. Qiao, *ACS Nano* **2014**, *8*, 5290; f) Z. Y. Jin, A. H. Lu, Y. Y. Xu, J. T. Zhang, W. C. Li, *Adv. Mater.* **2014**, *26*, 3700.

[2] a) S. H. Joo, S. J. Choi, I. Oh, J. Kwak, Z. Lin, O. Terasaki, R. Ryoo, *Nature* **2001**, *412*, 169; b) J. H. Bang, K. Han, S. E. Skrabalak, H. Kim, K. S. Suslick, *J. Phys. Chem. C* **2007**, *111*, 10959; c) H. D. Du, L. Gan, B. H. Li, P. Wu, Y. L. Qiu, F. Y. Kang, R. W. Fu, Y. Q. Zeng, *J. Phys. Chem. C* **2007**, *111*, 2040; d) J. Tang, J. Liu, N. L. Torad, T. Kimura, Y. Yamauchi, *Nano Today* **2014**, *9*, 305.

[3] a) J. Liu, T. Y. Yang, D. W. Wang, G. Q. Lu, D. Y. Zhao, S. Z. Qiao, *Nat. Commun.* **2013**, *4*, 2798; b) X. Sun, Y. D. Li, *Angew. Chem. Int. Ed.* **2004**, *43*, 597; *Angew. Chem.* **2004**, *116*, 607; c) A. H. Lu, G. P. Hao, Q. Sun, *Angew. Chem. Int. Ed.* **2011**, *50*, 9023; *Angew. Chem.* **2011**, *123*, 9187; d) A. H. Lu, T. Sun, W. C. Li, Q. Sun, F. Han, D. H. Liu, Y. Guo, *Angew. Chem. Int. Ed.* **2011**, *50*, 11765; *Angew. Chem.* **2011**, *123*, 11969.

[4] a) Z. A. Qiao, B. K. Guo, A. J. Binder, J. H. Chen, G. M. Veith, S. Dai, *Nano Lett.* **2013**, *13*, 207; b) N. P. Wickramaratne, J. T. Xu, M. Wang, L. Zhu, L. M. Dai, M. Jaroniec, *Chem. Mater.* **2014**, *26*, 2820; c) Y. Fang, G. F. Zheng, J. P. Yang, H. S. Tang, Y. F. Zhang, B. Kong, Y. Y. Lv, C. J. Xu, A. M. Asiri, J. Zi, F. Zhang, D. Y. Zhao, *Angew. Chem. Int. Ed.* **2014**, *53*, 5366; *Angew. Chem.* **2014**, *126*, 5470.

[5] a) S. Wang, W. C. Li, G. P. Hao, Y. Hao, Q. Sun, X. Q. Zhang, A. H. Lu, *J. Am. Chem. Soc.* **2011**, *133*, 15304; b) J. Liu, S. Z. Qiao, H. Liu, J. Chen, A. Orpe, D. Y. Zhao, G. Q. Lu, *Angew. Chem. Int. Ed.* **2011**, *50*, 5947; *Angew. Chem.* **2011**, *123*, 6069; c) J. Choma, D. Jamiola, K. Augustynek, M. Marszewski, M. Gao, M. Jaroniec, *J. Mater. Chem.* **2012**, *22*, 12636.

[6] a) K. Ai, Y. L. Liu, C. P. Ruan, L. H. Lu, G. Q. Lu, *Adv. Mater.* **2013**, *25*, 998; b) Y. Fang, D. Gu, Y. Zou, Z. X. Wu, F. Y. Li, R. C. Che, Y. H. Deng, B. Tu, D. Y. Zhao, *Angew. Chem. Int. Ed.* **2010**, *49*, 7987; *Angew. Chem.* **2010**, *122*, 8159.

[7] a) C. Liang, K. Hong, G. A. Guiochon, J. M. Mays, S. Dai, *Angew. Chem. Int. Ed.* **2004**, *43*, 5785; *Angew. Chem.* **2004**, *116*, 5909; b) Y. H. Deng, J. Wei, Z. K. Sun, D. Y. Zhao, *Chem. Soc. Rev.* **2013**, *42*, 4054; c) Y. H. Deng, C. Liu, D. Gu, T. Yu, B. Tu, D. Y. Zhao, *J. Mater. Chem.* **2008**, *18*, 91; d) H. I. Lee, J. H. Kim, D. J. You, J. E. Lee, J. M. Kim, W. S. Ahn, C. Pak, S. H. Joo, H. Chang, D. Seung, *Adv. Mater.* **2008**, *20*, 757.

[8] a) R. Liu, S. M. Mahurin, C. Li, R. R. Unocic, J. C. Idrobo, H. Gao, S. J. Pennycook, S. Dai, *Angew. Chem. Int. Ed.* **2011**, *50*, 6799; *Angew. Chem.* **2011**, *123*, 6931; b) F. W. Ma, H. Zhao, L. P. Sun, Q. Li, L. H. Huo, T. Xia, S. Gao, G. S. Pang, Z. Shi, S. H. Feng, *J. Mater. Chem.* **2012**, *22*, 13464; c) J. Sun, J. Zhang, M. Zhang, M. Antonietti, X. Fu, X. Wang, *Nat. Commun.* **2012**, *3*, 1139; d) J. Yan, L. Yang, M. F. Lin, J. Ma, X. Lu, P. S. Lee, *Small* **2013**, *9*, 596.

[9] a) X. H. Li, M. Antonietti, *Angew. Chem. Int. Ed.* **2013**, *52*, 4572; *Angew. Chem.* **2013**, *125*, 4670; b) T. Wang, C. X. Zhang, X. Sun, Y. X. Guo, H. Guo, J. Tang, H. R. Xue, M. Z. Liu, X. X. Zhang, L. Zhu, Q. Q. Xie, J. P. He, *J. Power Sources* **2012**, *212*, 1; c) Z. W. Liu, F. Peng, H. J. Wang, H. Yu, W. X. Zheng, J. Yang, *Angew. Chem. Int. Ed.* **2011**, *50*, 3257; *Angew. Chem.* **2011**, *123*, 3315; d) Y. Q. Chang, F. Hong, C. X. He, Q. L. Zhang, J. H. Liu, *Adv. Mater.* **2013**, *25*, 4794.

[10] a) H. Lee, S. M. Dellatore, W. M. Miller, P. B. Messersmith, *Science* **2007**, *318*, 426; b) S. Hong, Y. S. Na, S. Choi, I. T. Song, W. Y. Kim, H. Lee, *Adv. Funct. Mater.* **2012**, *22*, 4711; c) F. Q. Zhang, Y. Meng, D. Gu, Y. Yan, C. Z. Yu, B. Tu, D. Y. Zhao, *J. Am. Chem. Soc.* **2005**, *127*, 13508.

[11] R. J. Li, K. Parvez, F. Hinkel, X. L. Feng, K. Müllen, *Angew. Chem. Int. Ed.* **2013**, *52*, 5535; *Angew. Chem.* **2013**, *125*, 5645.

[12] E. Raymundo-Piñero, D. Cazorla-Amorós, A. Linares-Solano, J. Find, U. Wild, R. Schlögl, *Carbon* **2002**, *40*, 597.

[13] M. C. Huang, H. S. Teng, *Carbon* **2003**, *41*, 951.

[14] C. Weidenthaler, A. H. Lu, W. Schmidt, F. Schüth, *Microporous Mesoporous Mater.* **2006**, *88*, 238.

[15] a) K. P. Gong, F. Du, Z. H. Xia, M. Durstock, L. M. Dai, *Science* **2009**, *323*, 760; b) R. L. Liu, D. Q. Wu, X. L. Feng, K. Müllen, *Angew. Chem. Int. Ed.* **2010**, *49*, 2565; *Angew. Chem.* **2010**, *122*, 2619; c) L. F. Lai, J. R. Potts, D. Zhan, L. Wang, C. K. Poh, C. H. Tang, H. Gong, Z. X. Shen, J. Y. Lin, R. S. Ruoff, *Energy Environ. Sci.* **2012**, *5*, 7936; d) D. H. Deng, X. L. Pan, L. A. Yu, Y. Cui, Y. P. Jiang, J. Qi, W. X. Li, Q. A. Fu, X. C. Ma, Q. K. Xue, G. Q. Sun, X. H. Bao, *Chem. Mater.* **2011**, *23*, 1188; e) P. Wang, Z. K. Wang, L. X. Jia, Z. L. Xiao, *Phys. Chem. Chem. Phys.* **2009**, *11*, 2730.

[16] a) G. S. Chai, I. S. Shin, J. S. Yu, *Adv. Mater.* **2004**, *16*, 2057; b) S. An, J. H. Park, C. H. Shin, J. Joo, E. Ramasamy, J. Hwang, J. Lee, *Carbon* **2011**, *49*, 1108; c) B. Z. Fang, J. H. Kim, M. Kim, J. S. Yu, *Chem. Mater.* **2009**, *21*, 789; d) B. Z. Fang, J. H. Kim, C. Lee, J. S. Yu, *J. Phys. Chem. C* **2008**, *112*, 639; e) J. Liang, Y. Zheng, J. Chen, J. Liu, D. Hulicova-Jurcakova, M. Jaroniec, S. Z. Qiao, *Angew. Chem. Int. Ed.* **2012**, *51*, 3892; *Angew. Chem.* **2012**, *124*, 3958.

[17] Y. Jiao, Y. Zheng, M. Jaroniec, S. Z. Qiao, *J. Am. Chem. Soc.* **2014**, *136*, 4394.

[18] a) D. S. Yang, D. Bhattacharjya, S. Inamdar, J. Park, J. S. Yu, *J. Am. Chem. Soc.* **2012**, *134*, 16127; b) P. Chen, T. Y. Xiao, Y. H. Qian, S. S. Li, S. H. Yu, *Adv. Mater.* **2013**, *25*, 3192; c) M. K. Liu, Y. F. Song, S. X. He, W. W. Tjiu, J. S. Pan, Y. Y. Xia, T. X. Liu, *ACS Appl. Mater. Interfaces* **2014**, *6*, 4214; d) J. Yan, H. Meng, W. D. Yu, X. L. Yuan, W. R. Lin, W. P. Ouyang, D. S. Yuan, *Electrochim. Acta* **2014**, *129*, 196.

[19] a) S. Wang, L. Zhang, Z. Xia, A. Roy, D. W. Chang, J. B. Baek, L. Dai, *Angew. Chem. Int. Ed.* **2012**, *51*, 4209; *Angew. Chem.* **2012**, *124*, 4285; b) J. Tang, T. Wang, X. C. Pan, X. Sun, X. L. Fan, Y. X. Guo, H. R. Xue, J. P. He, *J. Phys. Chem. C* **2013**, *117*, 16896.

[20] S. S. Feng, W. Li, Q. Shi, Y. H. Li, J. C. Chen, Y. Ling, A. M. Asiri, D. Y. Zhao, *Chem. Commun.* **2014**, *50*, 329.

